z- and ρ-AMOC under pre-industrial, historical and abrupt4xCO_2 climates in AWI-ESM2.1

F. D. A. O. Matos[1], D. Sidorenko[1], P. Gierz[1], X. Shi[1], L. Ackermann[1], G. Lohmann[12]

[1]Alfred Wegener Institute, Helmholtz centre for polar and Marine Research, Bremerhaven, Germany
[2]Department of Environmental Physics and MARUM, University of Bremen, Bremen, Germany

Key Points:

- The AMOC patterns from pre-industrial to historical climates differ considerably between density and constant depth frameworks
- ρ-AMOC provides a more physical representation of deep convection and allow for analysis of water mass transformations
- AMOC is abruptly weakened and then recovers mostly due to surface-forced diapycnal transformations under 4xCO_2 forcing

Corresponding author: Fernanda Matos, fernanda.matos@awi.de

Abstract

The Atlantic Meridional Overturning Circulation (AMOC) is one of the most essential mechanisms influencing our climate system. By comparing constant depth (z-AMOC) and density (ρ-AMOC) frameworks under pre-industrial, historical and abrupt 4xCO_2 scenarios we analyze how the circulation mean state and variability differ amongst them. Water mass transformations are also assessed as a matter of analyzing surface-induced and interior-mixing-induced transformations. As expected, both location and strength of AMOC maxima are deeply affected by the framework choice, with the AMOC reaching a maximum transport of 21 Sv at around 35 °N under constant depth coordinates, as opposed to $\sim$ 25 Sv at 55 °N when diagnosed from density surfaces for both pre-industrial and historical climate. When quadrupling the CO_2, both frameworks exhibit an abrupt AMOC weakening followed by a steady recovery to maximum values of 10-15Sv. The z-AMOC maxima timeseries correlates more with those at 26 °N (r $\sim$0.7) than with the ρ-AMOC maxima (r $\sim$-0.3), due to the flatter isopycnals in the z framework even in the subpolar North Atlantic, where isopycnals are, in fact, steeper. Based on this discrepancy, we argue that the density framework is more coherent to the physics of this circulation by directly incorporating water mass transformations and their density structure. We suggest that more analysis across timescales and under different conditions must be performed with density surface outputs being provided by as many models as possible, to enable a more comprehensive analysis of these two frameworks and their applications.

Plain Language Summary

The global ocean circulation is largely responsible for inter-hemispheric transport of several properties in the form of ocean currents and water masses that occupy different density classes in the water column. Its branch in the Atlantic Ocean, the Atlantic Meridional Overturning Circulation (AMOC) is deemed to have a larger role in this process, driving feedbacks that strongly influence climate change across timescales. In Climate and Earth System Models, the AMOC strength is calculated over a period of time using different horizontal and vertical resolutions, mainly by averaging the water column in constant depth intervals (z-AMOC). However, as the ocean isopycnals are steeper where deep convection occurs, we argue that studying the AMOC should include an analysis of its state and variability by calculating this circulation as a function of density and latitude (ρ-AMOC). To support our claim, we performed simulations under pre-industrial and historical forcing and in a scenario where the CO_2 concentrations were quadrupled (4xCO_2). From our results, we indicate that ρ-AMOC provides more physical and meaningful information about the AMOC strength, stability, and water mass transformations, and we suggest further analysis that can contribute to our understanding of the underlying mechanisms driving this circulation.

1 Introduction

The Atlantic Meridional Overturning Circulation (AMOC) is considered one of the tipping elements of the Earth's system, as it is responsible for approximately 25% of the global heat transport and for up to half of the deep-water formation in the ocean (Srokosz et al., 2012). Therefore, investigating its underlying mechanisms has become of particular importance as it is essential to understand climate change across timescales and under different scenarios, as well as climate extremes (Bellomo et al., 2021). These factors among others are responsible for the boosted interest and investment in developing research about the AMOC strength and variability over the past decades.

From a simplified definition, the AMOC consists firstly of an upper limb of warm and saline waters moving towards the subpolar North Atlantic (Broecker, 1987). This limb is established from two main pathways, the so-called cold and warm routes. The

cold route is supplied by the cold and fresh waters entering the Atlantic from the Drake Passage, in the Southern Ocean, whereas the warm route is supplied by relatively warm and salty waters injected into the Atlantic from the Agulhas Leakage region, on the connection between the Indian and Atlantic oceans (Rühs et al., 2019). The maximum northward transport is observed in its mid-depth cell, around 1200 meters depth, within 30°N to 65°N (McCarthy et al., 2017). When the waters composing the upper limb reach the northern North Atlantic, because of heat loss to the atmosphere and subsequent buoyancy loss (density gain), it sinks and returns southwards as a cold and dense lower limb, mostly represented by the North Atlantic Deep Water (NADW) (Cheng et al., 2013; Buckley & Marshall, 2016).

The AMOC strength and variability are driven by buoyancy fluxes and interior mixing augmented by cabbeling and thermobaricity. Therefore, they critically depend on fluctuations in the heat and freshwater fluxes along the Atlantic Ocean which control the density of the water masses being transported by ocean currents (Sévellec & Fedorov, 2016).

The AMOC variability includes decadal, and centennial to millennial scales (Marson et al., 2014), making its analysis rather untrivial, especially if one considers that the current observational arrays are somewhat limited as they still lack temporal resolution and are biased by the natural variability of the system (Frajka-Williams et al., 2019). Moreover, observing the Earth at a fine spatial resolution is not yet feasible. Hence for the analysis of the paleo, current, and future climate simulations the researchers often resort to numerical model simulations.

Owing to the necessity of improving the hierarchy of models available for climate research, many institutions started to develop their own Coupled and Earth System Models (CMs and ESMs, respectively), and a project which could foster a common framework for climate research became necessary. In this sense, the Coupled Model Intercomparison Project (CMIP) was initiated under the aegis of the World Climate Research Programme (WCRP). There is no doubt about the contribution of these models to the current understanding of climate processes and variability, especially under the latest CMIP phase (CMIP6; (Eyring et al., 2016)). However, model uncertainties are still a caveat for decision-making towards adapting to and mitigating climate change once they reduce the confidence in the results presented.

The most common limitations leading to model uncertainty in several aspects are biases resulting from their parameterizations and resolutions. If on one hand high-resolution models are capable of simulating smaller-scale processes, they are still largely constrained by the temporal scale and computational cost. The models allowing for simulations across longer timescales are often configured at a coarse resolution, which can sacrifice processes that rely heavily on eddy variability, for example (Hirschi et al., 2020; Chassignet et al., 2020). Overall, the methodology used to study the climate will depend on the scope of each research, limitations, and concessions which can be made. In addition, several gaps still need to be filled, such as the widely-known poorly prescribed cloud coverage by many models which imposes unusual precipitation patterns over the eastern basins, thus influencing sea surface salinity and freshwater fluxes in these regions (Reintges et al., 2017; Stouffer et al., 2017; Foltz et al., 2019).

Another point for consideration is the choice of vertical coordinates. For most CMIP model output, the ocean dynamics are represented under constant depth coordinates, and therefore the AMOC is calculated as a zonally averaged stream function varying in latitude and constant depth intervals (z-AMOC hereafter)(Mecking et al., 2017). Even though this representation may be more straightforward than others, the AMOC variability is primarily driven by water mass transformations towards deep convection in the subpolar Atlantic, where most oceanic flows follow inclined isopycnal surfaces. Thus, this circulation would be better defined as a function of density and latitude (ρ-AMOC here-

after) (Sidorenko, Danilov, Fofonova, et al., 2020; Xu et al., 2018; Megann, 2018; Johnson et al., 2019).

Considering both frameworks, the representation of the ocean under density surfaces offers the advantage of directly accounting for water mass transformations (Desbruyères et al., 2019), while averaging the ocean in constant depths may lead to the formation of spurious cells (such as the Deacon cell in the Southern Ocean; see Döös and Webb (1994); D. P. Stevens and Ivchenko (1997); Speer et al. (2000)), and the highly discussed discrepancy between models and observations on the AMOC stability. Even though both agree that the AMOC is weakening in the current decade, the magnitude of this weakening is higher in observations. Under the current climate model results, the AMOC is often too strong, probably because of a misrepresentation of deep convection as a consequence of large salinity biases masking the effect of increasing meltwater input in the subpolar North Atlantic due to climate change (Liu et al., 2017).

Here we investigate the AMOC mean state and variability under two different frameworks by a suite of simulations conducted with AWI-ESM2.1 (Alfred Wegener Institute Earth System Model version 2.1). AWI-ESM2.1 performs the diagnostics in both frameworks online, which advances this methodology over previous studies (Sidorenko et al., 2021).

This manuscript is organized as follows: section 2 describes the methodology employed in the simulations, section 3 is dedicated to explaining the AMOC mean state and variability, and section 4 the water mass transformations. The discussion on the most critical questions arising from the results is presented in section 5, followed by the conclusions in section 6.

2 Methodology

2.1 Model description and simulation setup

Pre-industrial, historical and 4xCO_2 simulations of AMOC under density surface (ρ-AMOC) and constant depth (z-AMOC) coordinates were performed with AWI-ESM2.1 (Sidorenko et al., 2015; Rackow et al., 2018). It is built under the modular framework of ESM-tools software (Barbi et al., 2021), which allows for the reuse of the developments in several contexts regardless of the lifespan of the model components. This model configuration includes ECHAM6.3 (B. Stevens et al., 2013) as the atmospheric component, and FESOM2.1 (Finite-volumE Sea ice-Ocean Model version 2.1; (Danilov et al., 2017; Sidorenko et al., 2019; Scholz et al., 2019; Koldunov et al., 2019; Scholz et al., 2022)) as the ocean and ice component. In its modular framework, the AWI-ESM2.1 model components are coupled by the OASIS3-MCT coupler (Valcke, 2013; Craig et al., 2017) with ECHAM6.3 computing 12 air-sea fluxes based on four surface fields provided by FESOM2.1, while OASIS3-MCT maps the mean fields and accumulated fluxes between the model components every 6 hours.

ECHAM6.3 is mainly developed by the Max Planck Institute for Meteorology (MPI-M) and is focused on the coupling of processes driven by radiative forcing such as diabatic processes and large-scale circulations. In AWI-ESM2.1, the gaussian grid configuration T63L47 of ECHAM is employed, with a horizontal spectral resolution of about 1.9° and 47 vertical levels, which is one of the few configurations providing a stable climate when coupled with ocean models (Giorgetta et al., 2013). It also includes a land surface model, JSBACH (Raddatz et al., 2007), providing interactive vegetation dynamics.

FESOM2.1, developed by Alfred Wegener Institute, is a hydrostatic ocean and ice circulation model built on triangular unstructured meshes and under a finite volume approach, enabling simulations with variable resolution without the need for nesting and

with a higher computer efficiency (Shi et al., 2020). In FESOM2.1, the mesh is configured with a nominal one-degree resolution in the ocean interior, becoming finer towards the Equator and north of 50°N, where it reaches 1/3° and 24 km, respectively, and the ocean surface is discretized in about 127,000 grid points. The vertical resolution is distributed in 46 depth levels under an Arbitrary-Lagrangian-Eulerian (ALE) vertical coordinate scheme, which allows for the application of distinct vertical layers. In this simulation, the z* vertical coordinate is employed, enabling the reduction of spurious mixing by scaling the vertical coordinate in proportion to sea surface height (Petersen et al., 2015).

For the online diagnostic of AMOC in density classes, the model vertical levels are remapped onto 85 density bins (ρ-bins) referenced to 2000 dbar (σ^2; $\mathrm{kg\,m^{-3}}$) and ranging from 30-40$\mathrm{kg\,m^{-3}}$, following the description of Megann (2018), Xu et al. (2018) and Sidorenko, Danilov, Fofonova, et al. (2020).

The Pre-industrial (PI) control simulation employed here consists of a 1300 year integration of model components under an external forcing from the year 1850, where only the last 300 years were used for analysis. Additionally, the historical and the 4xCO_2 simulations were initialised from the final state of the PI run from 1850, according to CMIP standards.

The simulations were performed to provide all the usual variables as an output in addition to the transports in density space. The fact that these computations were performed simultaneously during run time diminishes computational costs and storage needs (Sidorenko et al., 2021).

2.2 Mathematical framework

In addition to ρ-AMOC, the contributions from surface-induced diapycnal and interior-mixing-induced water mass transformations to the AMOC (referred to as surface and interior transformations hereafter), as well as the volume drift between density classes are also calculated. z-AMOC, ρ-AMOC, and surface and internal transformations are calculated following Sidorenko, Danilov, Fofonova, et al. (2020) mathematical framework, using the algorithms for AMOC on unstructured meshes described in Sidorenko, Danilov, Koldunov, et al. (2020). We only provide some basic definitions here for the sake of completeness. Thus, ρ-AMOC is defined according to Eq. 1 below:

$$\psi_\sigma(y,\rho) = \int_{North}^{y}\int_{East}^{West} w_p(x',y',\rho')dx'dz' \tag{1}$$

Where w_p corresponds to the diapycnal velocity across the density surface ρ, and is obtained through reconstruction from the divergence of horizontal flow within each density bin. Even though ρ-AMOC can also be calculated with the meridional velocity, using diapycnal velocity instead is deemed to be more convenient for online diagnostic computation, less noisy and directly connected to water mass transformations (Sidorenko, Danilov, Fofonova, et al., 2020).

In order to calculate internal transformations ψ_I, it is first necessary to calculate the total diapycnal transport, ψ_T, and the surface-forced transformation, ψ_S, once the first is the result of the difference between the two latest, according to the following Eqs. 2, 3, 4:

$$\psi_T(y,\rho) = \psi_\sigma(y,\rho) - \frac{\Delta V}{\Delta t} \tag{2}$$

$$\psi_S(y,\rho) = \frac{1}{\Delta\rho}\int_{West}^{East}\int_{North}^{y}\int_{\rho+\frac{\delta\rho}{2}}^{\rho-\frac{\delta\rho}{2}} F_p(x',y',\rho')d\rho' dy' dx' \tag{3}$$

$$\psi_I(y,\rho) = \psi_\sigma(y,\rho) - \frac{\Delta V}{\Delta t} - \psi_S(y,\rho) \tag{4}$$

where F_P is the buoyancy flux, $\Delta\rho$ is the size of the density bin and $\Delta V/\Delta t$ represents the model drift (i.e. rate of volume change over time). According to the same rationale, z-AMOC is also calculated using vertical velocity (w), following the Eq. 5 below:

$$\psi_z(y,z) = \int_{North}^{y}\int_{-\pi}^{\pi} w(x,y',z')dx' dy' \tag{5}$$

3 AMOC mean state and variability

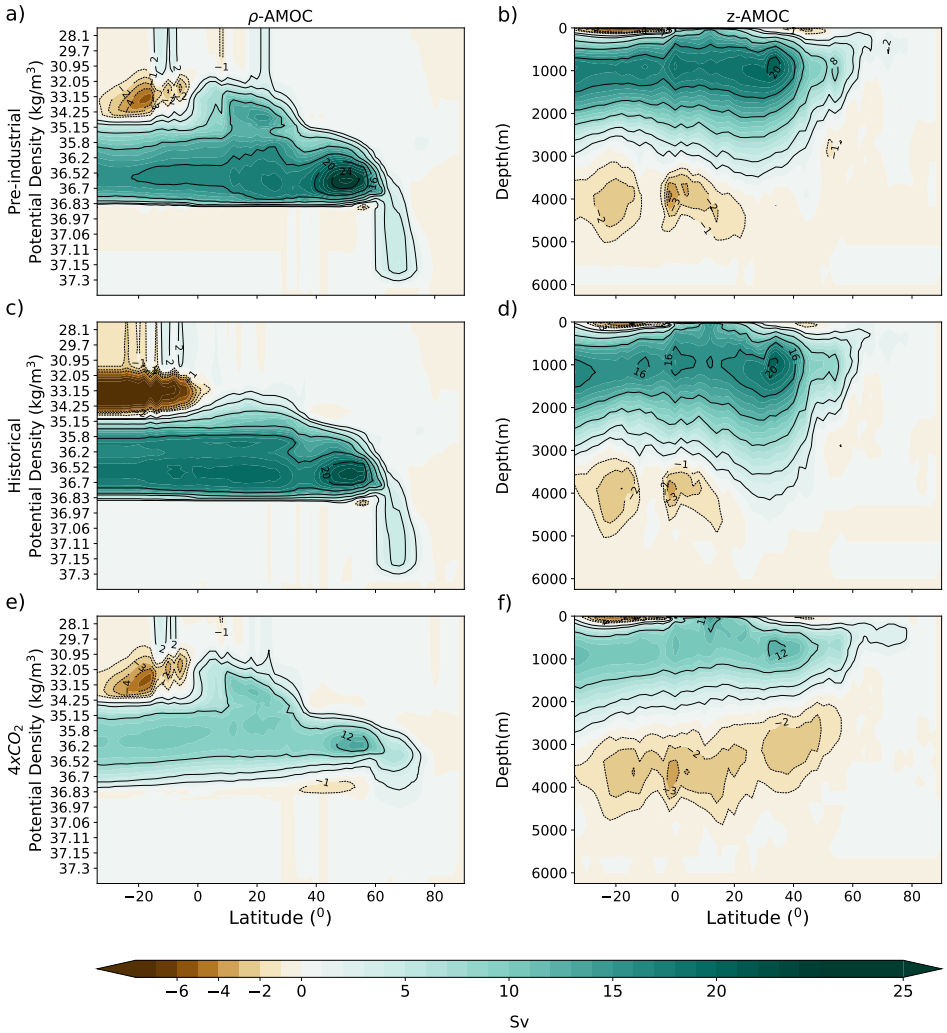

Figure 1. Mean AMOC strength for pre-industrial a) ρ - and b) z-AMOC, historical c) ρ- and d) z-AMOC and e) ρ- and f) z-AMOC.

Figures 1a, c, and e display ρ-AMOC (ψ_σ) for pre-industrial, historical and 4xCO_2 scenarios, respectively. Overall, ψ_σ is characterised by a mid-depth cell associated with NADW that flows southward as the AMOC lower limb. This cell is centered at around $36.62\,\mathrm{kg\,m^{-3}}$ with a mean strength of $\sim 25\,\mathrm{Sv}$, $22\,\mathrm{Sv}$ and $13\,\mathrm{Sv}$ at 50°N, 52°N and 56°N for pre-industrial, historical and 4xCO_2 runs, respectively, where water mass transformations resulting in deep convection tend to occur. A shallower secondary maximum near 20°N is also featured, representing the diapycnal component of the subtropical gyre. The bottom cell, however, representing the Antarctic Bottom Water (AABW) is not depicted and would be characterized by a cell centered around $37.15\,\mathrm{kg\,m^{-3}}$ reaching up to 20°N, even tough its magnitude is consistently small in previous studies (Xu et al., 2018; Sidorenko et al., 2021). Another feature depicted by Figures 1a, c, and e are the Nordic Seas Overflow Waters (NSOW), characterized by a large vertical extent of strong circulation from 60° to 80°N, as a result of its topographic limitations (Saunders, 2001).

Z-AMOC (ψ_z) is displayed in figures 1b, d, and e for pre-industrial, historical, and 4xCO_2 scenarios, respectively. Its middepth cell is centered at around 1000 m with a maximum at approximately 32°N of $\sim 21\,\mathrm{Sv}$ for pre-industrial and historical runs, and $\sim 12\,\mathrm{Sv}$ for the 4xCO_2 run. The bottom cell is centered at 4000 m with a strength of $\sim$ 2-4 Sv in all runs, however, this cell reaches up to 40°N when CO_2 concentrations are quadrupled.

The presence of a recirculation cell characterised by closed streamlines surrounding the AMOC maximum is common to both frameworks. However, the ρ-AMOC recirculation is shifted further North, between 45°N and 60°N when compared to z-AMOC, with the recirculation cell confined between 30°N and 45°N. Such displacement is typical for model results with constant-depth frameworks and coarse resolutions, such as most CMIP models, indicating that the biases which are present do not impair the consonance of the results when compared to other models of similar configuration (Xu et al., 2019).

Figure 2 provides meaningful information on the trend from pre-industrial to historical and 4xCO_2 forcing. In figure 2a, the ρ-AMOC trend is expressed by a weakening of the subpolar cell from 40-60°N and concurrent strengthening south of $\sim$ 30°N. The weakening is also prominent for both tropical and subpolar cells. On the other hand, figure 2b depicts an overall AMOC weakening in the first 1500 m, while it is strengthened below this level. Such strengthening is a result of a deepened NADW and a stronger AABW, instead of an actual increase in volume transport, as the magnitude of the circulation remains the same.

There is more consistency between trends in the two frameworks for 4xCO_2 (Figures 2c and d) scenarios where both show a weakening of the subpolar cells. This reduced strength is, however, more expressed in the density framework plots (Figure 2d).

The evaluation of AMOC variability can be performed following diverse modelling and observational approaches. Most studies with coupled-climate and earth system models compute AMOC at 3 different regions where observational arrays were also conducted over the past decade: (1) 34°S, the southernmost limit of the Atlantic and where the SAMBA array is located (Meinen et al., 2018), (2) between 30 to 65°N, where the circulation is deemed to be the strongest (Mecking et al., 2017; Matos et al., 2020), and the OSNAP array is developed (Lozier et al., 2017), and/or (3) 26.5°N, where the RAPID/MOCHA array is located (McCarthy et al., 2017). All approaches are used within the scope of the hypothesis presented, however, for this study two regions were chosen to describe the AMOC variability under both frameworks: the AMOC maxima, located at around 30°N for z-AMOC and 50°N for ρ-AMOC; and at 26°N to allow for comparisons with observations.

The time series (Figure 3) highlights that not only the location of the AMOC maxima but also the AMOC variability is affected by the choice of framework. The variabil-

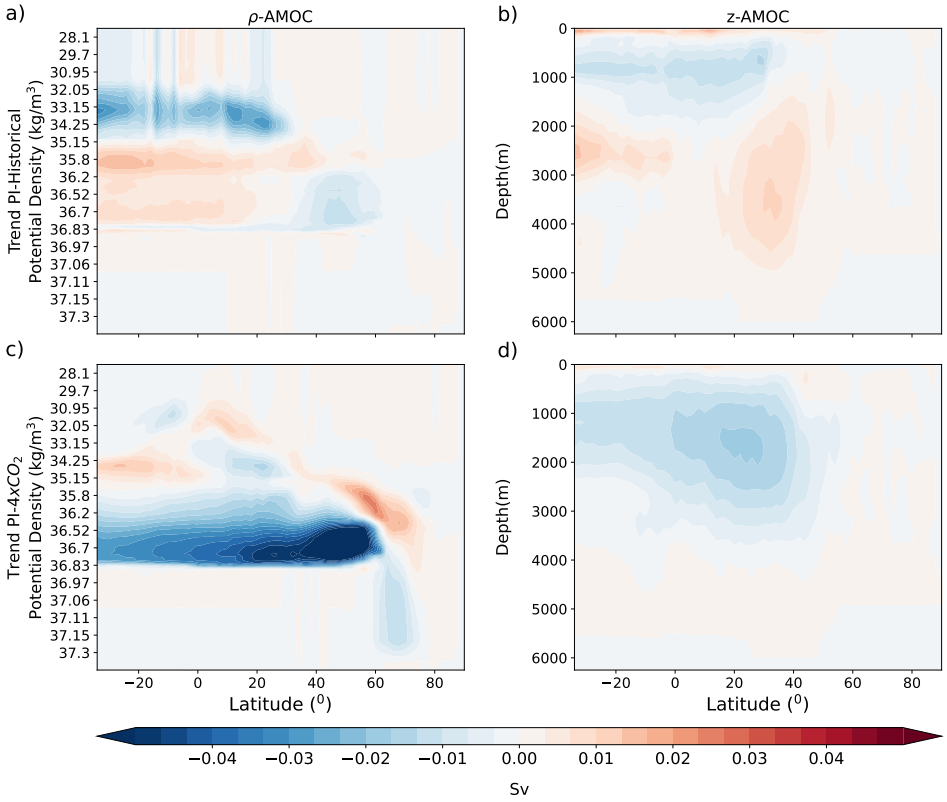

Figure 2. Mean AMOC strength for pre-industrial a) ρ - and b) z-AMOC, historical c) ρ - and d) z-AMOC and e) ρ - and f) z-AMOC.

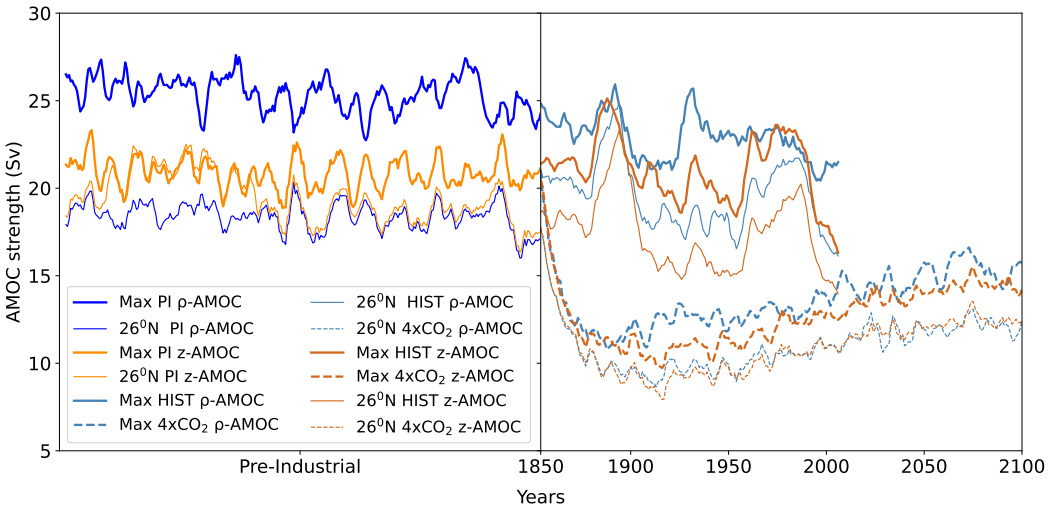

Figure 3. Annual mean time-series of ρ-AMOC (blue) and z-AMOC (orange) under pre-industrial, historical and 4xCO$_2$ forcing. The thicker lines represent the AMOC maxima, located at $\sim$ 32°N for depth and 50-56 °N for density frameworks, approximately.

ity under historical forcing is stronger compared to PI, as expected for such a transient forcing, and it is similar for z-AMOC maxima and the circulation at 26°N in both cases.

This reinforces the theory that z-AMOC displays a less significant weakening towards historical forcing than ρ-AMOC due to its maximum being located at a subtropical region, rather than it being a result of a decreased deep convection. On the other hand, the variability is strikingly similar for both frameworks under 4xCO_2 forcing (σ=$\sim$1.9), with an abrupt weakening during the first 50 years of simulation, followed by a steady recovery until the end of the century, still not sufficient to bring the AMOC strength to PI or historical levels.

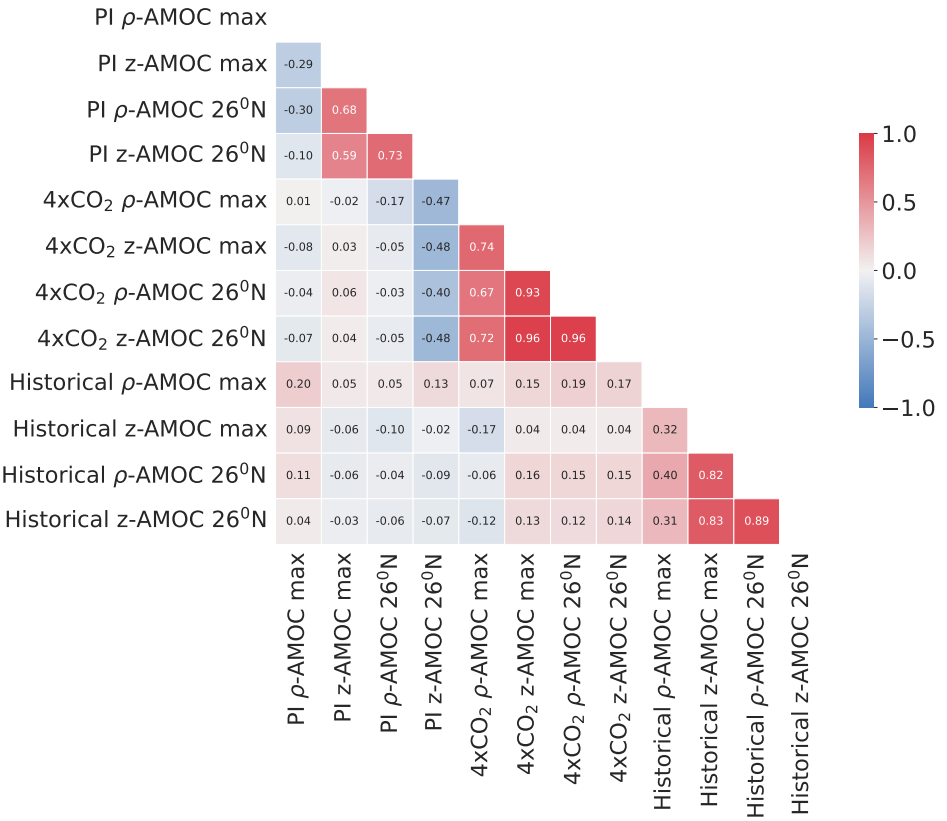

Figure 4. Correlation panel for both frameworks and under all forcing for the full time-series, at the AMOC maxima and at 26°N.

In terms of transport, ρ-AMOC is stronger compared with z-AMOC in the two regions considered. This pattern is expected, once the isopycnals in the subtropics are not so steep, therefore adopting a density approach to vertical coordinates imposes many differences and the results are similar to those of Sidorenko, Danilov, Fofonova, et al. (2020); Sidorenko et al. (2021) and Xu et al. (2018). This strongly indicates that even under different model configurations, the density surface approach is more suitable to explain the physics of the governing processes. Consequently, the AMOC maxima time series are not significantly correlated except under abrupt forcing, where the circulation enters a new regime. On the other hand, the time series of z- and ρ-AMOC at 26°N, and z-AMOC maxima are highly correlated (figure 4).

4 Surface-forced diapycnal and interior-mixing-induced water mass transformations

When inspecting the surface-forced diapycnal water mass transformations (ψ_S; Figures 5a, c, and e), one needs to consider that they reflect surface buoyancy fluxes and therefore only influence the surface mixed layer, therefore, it cannot be employed to track water masses (Xu et al., 2018). The pre-industrial pattern (Figure 5a) allows for the identification of three main cells within the limit of the upper limb: (1) the tropical cell centered at around $31.5\,\mathrm{kg\,m^{-3}}$, (2) the subtropical cell centered at $34.2\,\mathrm{kg\,m^{-3}}$, and (3) the subpolar cell centered at $36.8\,\mathrm{kg\,m^{-3}}$. The intermediate layer around $36.2\,\mathrm{kg\,m^{-3}}$ represents the Antarctic Intermediate Water (AAIW), formed in the Southern Ocean at intermediate density levels due to its low temperature/low salinity contrast (Santoso & England, 2004). This stratified pattern is important to provide information on the direction of the water mass transformation. The region to which each cell is attributed depends on the maximum reach.

Therefore, in the tropics, the surface-forced diapycnal transformations occur towards lighter waters, while in the subtropical and subpolar regions, they occur towards denser waters. When considering the role of the heat and freshwater fluxes in these buoyancy-driven transformations, heat fluxes drive these processes when compared with freshwater fluxes (not shown).

The interior-mixing-induced transformations (ψ_I; Figures 5 b, d, and f) account for water masses that are transformed by interior mixing and cabbeling after being advected from water masses modified by surface transformations. In a more simplified concept, it includes any water mass transformation which is not caused by air-sea buoyancy fluxes (Xu et al., 2018). These transformations are also affected by the model drift, once they are calculated by subtracting the total transformations from ψ_S. Especially for this simulation, the model drift is negligible, therefore, to compute the internal transformations, it was not considered.

The maximum of ψ_I located around the ρ-AMOC maxima indicates that the AMOC recirculation cell in pre-industrial (Figure 5b) and historical (Figure 5d) periods is substantially influenced by these transformations, even though the surface-forced diapycnal transformations still play a role by triggering mixing and consequent deep convection. On the other hand, the surface transformations are stronger in a more abrupt scenario (Figure 5f), becoming the maintainer of the overturning as the consequent mixing is not sufficient to create convection.

As an overall comparison between subpolar water mass transformations, both surface and interior transformations are directed downwards contributing to deep water formation. In subtropical regions, however, these transformations are directed towards lighter waters, contributing to the shallower secondary maxima occurring in this region. In the tropics, the surface-forced transformations are compensated by interior mixing resulting from the upwelling of the AMOC upper limb, resulting in an overall lighter circulation in this region. Additionally, in deeper waters, the interior mixing induced transformations occur towards denser water from 60-80°N, whereas towards lighter waters further south, triggering the formation of lighter NSOW which later contributes to the lower NADW cell.

As observed in Figure 5, these surface transformations can occur and trigger interior mixing at all density levels. As a way to visualize how and where these water mass transformations occur as a contribution to the AMOC under density surfaces or constant depth, figure 6 shows the surface transformations (Figures 6a, d, and g), diapycnal velocity (Figures 6b, e, and h), and vertical velocities (Figures 6c, f, and i) at the mid-depth cell location for each climate. These maps were conservatively remapped onto 4°x4° boxes

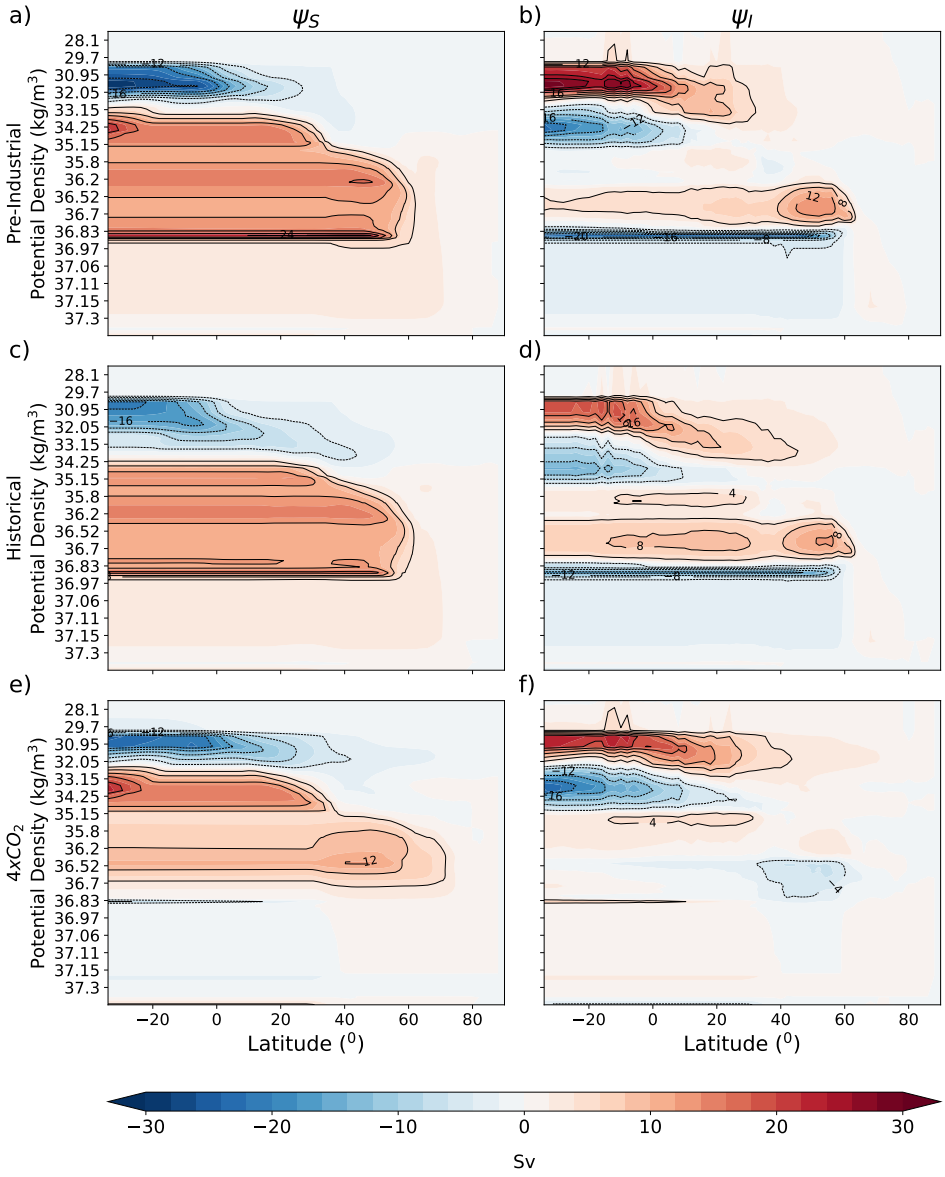

Figure 5. Mean surface-forced diapycnal water mass transformations (ψ_S) and interior-mixing-induced transformations (ψ_I) under pre-industrial (a and b), historical (c and d), and 4xCO_2 forcing (e and f), respectively

as the native grid would display a very noisy pattern, impairing the analysis of the governing processes.

Considering the pre-industrial forcing (Figures 6 a, b, and c), the pattern is qualitatively similar to that seen in Sidorenko et al. (2020) using the ocean-only simulation with CORE-II mesh. For surface transformations (Figure 6a), buoyancy loss (blue) is more prominent and seen at the Labrador and Irminger Seas (LS and IS, respectively) and along the Norwegian coast, whereas buoyancy gain (red) is not as strong and is confined to the east coast of Greenland and north of the Greenland-Scotland ridge. The combination of surface and interior transformations provides the pattern for total transformations, which are here depicted as diapycnal velocities (Figure 6b). In this sense, the

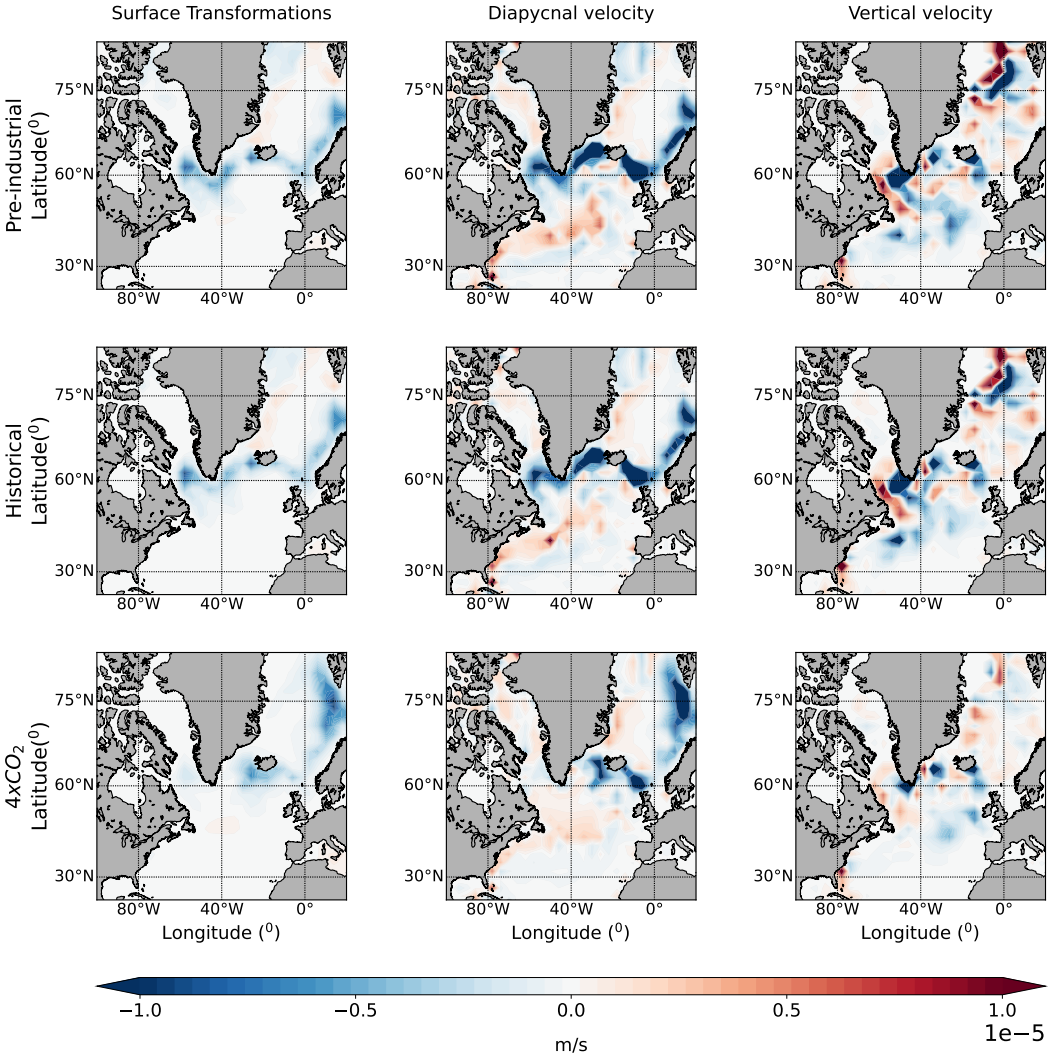

Figure 6. Mean surface-forced diapycnal water mass transformations (ψ_S), diapycnal velocity and vertical velocity at 1000 m, under pre-industrial (a, b, and c), historical (d, e, and f), and 4xCO_2 forcing (g, h and i), respectively. For surface transformations and diapycnal velocities, the density level differs between the forcing, being 36.62 kg m^{-3} for PI and historical and 36.02 kg m^{-3} for 4xCO_2 simulations

buoyancy loss pattern seen for surface transformations is converted into a larger downward flux but confined to the same regions.

However, there is considerable upward flux in the regions of Baffin Bay and following the Gulf Stream and North Atlantic Current routes, as well as in confined areas south of Iceland. Additionally, the isopycnal ρ=36.62 is shallower at the Labrador Sea compared to the eastern part of the North Atlantic subpolar gyre or further north, similar to the findings of (Lozier et al., 2019) using observational data from the OSNAP array.

The absence of surface transformations south of 50°N suggests that all transformations in this region at ρ=36.62 represent internal transformations, but the pattern shown for diapycnal velocities depicts a small but still noteworthy contribution of a downward flux. Finally, the pre-industrial vertical velocity at 1000 m (Figure 6c) displays a much

more noisy picture than that provided by ρ-AMOC water mass transformations. Even though there is a substantial contribution of South Greenland to z-AMOC, this downward flux is counteracted by upward fluxes in the Irminger and Labrador Seas. Additionally, although both frameworks depict upward flux at Cape Hatteras, the vertical velocity pattern shows downward flux along the Gulf Stream, related to the southward shift of the z-AMOC recirculation cell at this latitude, while for ρ-AMOC it is shifted further north.

The magnitude of the surface transformations and diapycnal and vertical velocities in the historical simulations is quite similar to that of the pre-industrial run. However, the surface transformations (Figure 6d) at the southern tip of Greenland become weaker, which results in a considerably decreased downward flux in this region and along the Norwegian coast, an eastward shift of the Gulf Stream, and a stronger downward flux along the eastern Labrador Sea. As the vertical velocity pattern (Figure 6f) is quite different from that shown in diapycnal velocity (Figure 6e), so is the historical configuration. The downward flux at the southern tip of Greenland and around the Gulf Stream is considerably stronger, in contrast to the eastern Atlantic, while there is a decrease in the upward flux seen at the eastern Labrador sea. Such a pattern can explain why the z-AMOC maxima remain around the same magnitude in PI and historical, with even a deepening of the lower cell seen in the latter, whereas ρ-AMOC weakens by 2-3Sv.

Comparing the $4xCO_2$ run to PI, the abrupt forcing causes a large AMOC weakening of around 12 Sv for the density surface framework and 8 Sv for the constant depth framework with both showing similar mechanisms being the main triggers. The diapycnal velocity (Figure 6h) plot shows a substantial decrease in the downward flux around the AMOC maxima (subpolar Atlantic) triggered by buoyancy loss in the LS, south Greenland and along the Norwegian coast. Buoyancy gain is seen in the eastern IS, which is also accompanied by an increase in the upward flux in the western region. An increased upward flux is also seen along the Gulf Stream. Figure 6i also indicates intense buoyancy loss in the Labrador Sea by a decrease in downward flux in the western LS and the opposite effect in the eastern LS. The downward flux around the AMOC maxima (subtropical Atlantic) is also decreased as in ρ-AMOC, indicating that the same mechanisms trigger AMOC weakening in both frameworks when under an abrupt forcing, resulting also in the shoaling of this circulation and a consequent northward shift of the AABW. This result also suggests that lower variability scenarios provide similar mechanisms for water mass transformations, even though the latitude difference between both frameworks remains a caveat for the calculation of AMOC under a constant depth framework.

5 Discussion

In this manuscript, we present an analysis of the Atlantic Meridional Overturning Circulation patterns and variability, as well as of water mass transformations, under constant depth (z framework) and density surfaces (ρ framework) as vertical coordinates. The comparison between frameworks is relevant because of two primary reasons: (1) the AMOC is driven by diapycnal transformations of the northward-flowing warm and saline waters into the southward flowing denser and colder North Atlantic Deep Water, and (2) the common constant depth coordinates provided by most climate and Earth System models do not account directly for these transformations. Therefore, the question of whether our current knowledge of processes underlying AMOC variability and stability is reliable arises, as most of what is known come from model output such as stream function and velocity components, both configured under constant depth vertical discretization, such as the majority of models contributing to CMIP6 (e.g., Weijer et al., 2020; Heuzé, 2021), and current observations are still too short-term for a more thorough analysis across timescales (Alkhayuon et al., 2019).

The results on ρ-AMOC and water mass transformations are consistent with previous studies using different models and resolutions (Xu et al., 2018; Roberts et al., 2020; Sidorenko, Danilov, Fofonova, et al., 2020; Sidorenko et al., 2021), which strengthens the hypothesis that computing the meridional overturning under density surfaces is able to depict the mechanisms driving the AMOC more coherently to the physics of mass transformations between density classes. Furthermore, it contributes to establishing this framework as an important tool for more refined climate research and advocating for the implementation of such output into other models, especially those participating in intercomparison projects and whose results are considered for political, economic, and societal decision-making under climate change conditions.

The patterns displayed in figure 3 also describe the physics of surface buoyancy fluxes to a coherent extent. Where the tropical cell is located in density class, the contributions from heat and freshwater fluxes are both directed towards lighter waters, indicating that the superficial water layer has a low salinity/high-temperature pattern, expected in such a warm region with high precipitation rates and strong runoff input. Within the subtropical cell, both act towards denser waters, revealing a saltier and colder surface ocean. In the subpolar region, however, the contribution of freshwater is too small compared to heat fluxes, and hardly counteracts its effect of mass transformations occurring towards denser waters.

The fact that these simulations cover different transient forcing scenarios compared to pre-industrial climate conditions allows for questions on how these freshwater and heat fluxes contributions could develop under climate change conditions. As mentioned before, the AMOC is deemed to be weakening due to the increase in freshwater forcing because of meltwater, and intensification of the hydrological cycle (Sévellec et al., 2017). This hypothesis comes from the so-called modes of AMOC stability, in which a strong AMOC would indicate a thermal regime where heat fluxes drive deep convection, and a weak AMOC would indicate a haline regime where a fresher subpolar North Atlantic would hamper deep water formation (Stommel, 1961; Alkhayuon et al., 2019). In these simulations, there is increased freshwater flux contribution to surface transformations in the subpolar cell from constant to transient forcing, even though it is significantly smaller than heat flux contributions. This indicates that a haline regime is unlikely to occur even under abrupt scenarios, but as the ocean is subjected to warming, at least in the subpolar North Atlantic, weaker heat and stronger freshwater flux contributions to the surface transformations are observed.

When considering the singularities of the upward/downward fluxes for each framework, the latitudinal band where strong downwelling and consequent deep water formation is considerably different, as seen in figure 6 but tied to similar mechanisms. The z-AMOC vertical velocity maps depict a downwelling along the path of the Gulf Stream and the North Atlantic Current, while in ρ-AMOC this process occurs along the subpolar gyre, mostly in the Labrador Sea and along the Norwegian coast, however, for both, it is associated with buoyancy gain. Under historical forcing, the dynamics of water transformations are fairly preserved, with a stronger buoyancy loss around the AMOC maxima occurring only when the circulation is calculated under density surfaces and a surprising increase in downward flux for z-AMOC resulting in AMOC deepening compared to PI. On the other hand, when CO_2 is quadrupled, intense buoyancy gain occurs around the AMOC maxima for both frameworks, resulting in weakening and shoaling of the circulation and a consequent northward shift of the Antarctic Bottom Water. This difference in where deep convection occurs at the density/depth level of the middepth cell results in z-AMOC maxima having similar variability to subtropical AMOC, regardless of how it is calculated. It is worth mentioning, however, that this characteristic arises not solely due to the fact that the isopycnals are flatter in subtropical regions but also because the same atmospheric forcing is employed.

It is also relevant to highlight that, as the variability of z-AMOC maxima is more correlated to subtropical AMOC, the density surface framework provides more insight into the region where massive water mass transformations take place in the North Atlantic and can be also useful for other studies which aim at calculating diapycnal mixing or transformations. AMOC in density space is also advantageous for studies concerning the meridional heat transport (MHT), as it is highly correlated in phase with ρ-AMOC at all latitudes. Especially in the subpolar gyre, it becomes even more important, as z-AMOC reveals a time lag with MHT (Kwon & Frankignoul, 2014).

Nevertheless, the fact that a constant depth framework is available as an output for several models extensively used for climate research, and that their AMOC computations are still consistent with observations beyond a reasonable doubt, does not discard its usefulness and robustness. Furthermore, the fact that the computation of ρ-AMOC requires high-frequency model output is a caveat that could not be overcome so far and could result in biased mesoscale processes (Sidorenko et al., 2021).

Another question that may arise is how the simulations performed in coarse resolution setups would be if a higher resolution would be applied (Haarsma et al., 2016; Hirschi et al., 2020; Roberts et al., 2020; Jackson et al., 2020). As displayed in figure 1, both frameworks feature a recirculation cell, which is actually deemed to be a result of spurious numerical mixing also imposed by the coarse resolution in this CORE-II mesh (Sidorenko et al., 2021; Xu et al., 2018).

In this case, even though the transport maximum is substantially higher for ρ-AMOC, previous analysis implementing higher resolution in FESOM standalone configuration shows that, because of a better representation of upwelling and water transformations at high latitudes, the ρ-AMOC northward transport could be even stronger and the recirculation cell driven by spurious mixing would disappear (Sidorenko, Danilov, Fofonova, et al., 2020). In this sense, the fact that AWI-ESM2.1 employs a modular framework with the ocean component built under unstructured meshes can represent an immense contribution toward higher resolution climate research. Such configuration allows for increased mesh resolution in regions of interest and should be also considered by other modeling centers.

Furthermore, it is noteworthy that an increase in resolution should not be limited to the oceanic component but also to atmospheric and other model components to allow for proper ventilation, for example (Sein et al., 2018).

6 Conclusion

Calculating the AMOC under density surfaces provides a better picture of water mass transformations, regions of deep convection, internal variability, and AMOC stability. The latitude range between 30-60°N is where most differences between z and ρ approaches lie, since the ρ-AMOC maxima of 25 Sv, is located at around 50°N while z-AMOC, on the other hand, has its maxima located far south, of 20 Sv at around 30°N. This latitudinal dependence dictates how the AMOC variability is depicted by each framework as the steeper isopycnals of the subpolar North Atlantic Ocean yield a higher sensitivity to different forcing mechanisms and a decadal variability pattern, while the subtropical ocean is more subjected to interannual variability, masking the trend exhibited by the time series.

As a result, the average ρ-AMOC maxima exhibit a stable circulation under PI forcing followed by an AMOC weakening of 2-5Sv under historical conditions, while z-AMOC strength remains at around 20 Sv for both scenarios.

Even though AMOC weakening is seen from PI to historical, it is not as strong as that under a more abrupt scenario, where both frameworks depict a sharp decrease of

8-12Sv in the first 50 years of simulation followed by a recovering to the end of the century until up to half of the PI levels. Such behavior is expected from previous analysis with not only this same forcing but also with future scenario approaches following different levels of radiative forcing.

The presence of recirculation cells also approximates these two frameworks, even though it is deemed to be an effect of coarse resolution and not of an alternative approach.

The results presented here shed light on several processes which account for AMOC variability and more consistent frameworks, however, some of the observations here discussed also indicate the necessity of further studies on biases caused by spurious mixing in different resolutions, the effect of model drift when computing transports, and more diagnostic approaches towards identifying the performance of this framework across different timescales, resolutions and forcing.

7 Data Availability Statement

The simulations with AWI-ESM2.1 were conducted under the framework of ESM-tools, an open-source software hosted on `https://github.com/esm-tools/esm_tools.git` with a modified GPLv2 licence. The ocean model FESOM2.1 source code is available at `https://github.com/FESOM/fesom2/releases/tag/2.1.0` with a GPL-3.0 licence. The OASIS coupler is available upon registration at: `https://oasis.cerfacs.fr/en/downloads/`. The source code for ECHAM6.3 as used in this study is not publicly available but rather subject to licencing by MPI-M Software Licence Agreement. The model results, as well as the postprocessing and visualisation scripts, are archived on Zenodo (Matos et al., 2022).

Acknowledgments
The work was supported by the Helmholtz climate initiatives REKLIM (Regional Climate Change) (Q. Wang and D. Sidorenko), and INSPIRES (International Science Program for Integrative Research in Earth Systems). The authors gratefully acknowledge the Jülich Supercomputing Centre (JSC) and the German Climate Computing Centre (DKRZ) for providing computing time on the supercomputers JUWELS and MISTRAL, respectively. We would also like to thank the Nippon Foundation and the Partnership for the Observation of the Global Ocean (POGO) for the support under the NF-POGO Centre of Excellence programme.

References

Alkhayuon, H., Ashwin, P., Jackson, L. C., Quinn, C., & Wood, R. A. (2019). Basin bifurcations, oscillatory instability and rate-induced thresholds for Atlantic meridional overturning circulation in a global oceanic box model. *Proceedings of the Royal Society A: Mathematical, Physical and Engineering Sciences*, *475*(2225), 20190051. doi: 10.1098/rspa.2019.0051

Barbi, D., Wieters, N., Gierz, P., Andrés-Martínez, M., Ural, D., Chegini, F., ... Cristini, L. (2021). ESM-Tools version 5.0: a modular infrastructure for stand-alone and coupled Earth system modelling (ESM). *Geoscientific Model Development*, *14*(6), 4051–4067. doi: 10.5194/gmd-14-4051-2021

Bellomo, K., Angeloni, M., Corti, S., & von Hardenberg, J. (2021). Future climate change shaped by inter-model differences in Atlantic meridional overturning circulation response. *Nature Communications*, *12*(1), 3659. doi: 10.1038/s41467-021-24015-w

Broecker, W. S. (1987). *The biggest chill: when ocean currents shifted, Europe suddenly got cold; could it happen again?* New York: American Museum of Natural History.

Buckley, M. W., & Marshall, J. (2016). Observations, inferences, and mechanisms of the Atlantic Meridional Overturning Circulation: A review. *Reviews of Geophysics*, *54*, 5–63. doi: 10.1002/2015RG000493

Chassignet, E. P., Yeager, S. G., Fox-Kemper, B., Bozec, A., Castruccio, F., Danabasoglu, G., ... Xu, X. (2020). Impact of horizontal resolution on global ocean–sea ice model simulations based on the experimental protocols of the Ocean Model Intercomparison Project phase 2 (OMIP-2). *Geoscientific Model Development*, *13*(9), 4595–4637. doi: 10.5194/gmd-13-4595-2020

Cheng, W., Chiang, J. C. H., & Zhang, D. (2013). Atlantic Meridional Overturning Circulation (AMOC) in CMIP5 Models: RCP and Historical Simulations. *Journal of Climate*, *26*(18), 7187–7197. doi: 10.1175/JCLI-D-12-00496.1

Craig, A., Valcke, S., & Coquart, L. (2017). Development and performance of a new version of the OASIS coupler, OASIS3-MCT_3.0. *Geoscientific Model Development*, *10*(9), 3297–3308. doi: 10.5194/gmd-10-3297-2017

Danilov, S., Sidorenko, D., Wang, Q., & Jung, T. (2017). The Finite-volumE Sea ice–Ocean Model (FESOM2). *Geoscientific Model Development*, *10*(2), 765–789. doi: 10.5194/gmd-10-765-2017

Desbruyères, D. G., Mercier, H., Maze, G., & Daniault, N. (2019). Surface predictor of overturning circulation and heat content change in the subpolar North Atlantic. *Ocean Science*, *15*(3), 809–817. doi: 10.5194/os-15-809-2019

Döös, K., & Webb, D. J. (1994). The Deacon Cell and the Other Meridional Cells of the Southern Ocean. *Journal of Physical Oceanography*, *24*(2), 429–442. doi: 10.1175/1520-0485(1994)024⟨0429:TDCATO⟩2.0.CO;2

Eyring, V., Bony, S., Meehl, G. A., Senior, C. A., Stevens, B., Stouffer, R. J., & Taylor, K. E. (2016). Overview of the Coupled Model Intercomparison Project Phase 6 (CMIP6) experimental design and organization. *Geoscientific Model Development*, *9*(5), 1937–1958. doi: 10.5194/gmd-9-1937-2016

Foltz, G. R., Brandt, P., Richter, I., Rodríguez-Fonseca, B., Hernandez, F., Dengler, M., ... Reul, N. (2019). The Tropical Atlantic Observing System. *Frontiers in Marine Science*, *6*. doi: 10.3389/fmars.2019.00206

Frajka-Williams, E., Ansorge, I. J., Baehr, J., Bryden, H. L., Chidichimo, M. P., Cunningham, S. A., ... Wilson, C. (2019). Atlantic Meridional Overturning Circulation: Observed Transport and Variability. *Frontiers in Marine Science*, *6*. doi: 10.3389/fmars.2019.00260

Giorgetta, M. A., Roeckner, E., Mauritsen, T., Bader, J., Crueger, T., Esch, M., ... Stevens, B. (2013). The atmospheric general circulation model ECHAM6 - Model description. (Publisher: Max-Planck-Institut für Meteorologie) doi: 10.17617/2.1810480

Haarsma, R. J., Roberts, M. J., Vidale, P. L., Senior, C. A., Bellucci, A., Bao, Q., ... von Storch, J.-S. (2016). High Resolution Model Intercomparison Project (HighResMIP v1.0) for CMIP6. *Geoscientific Model Development*, *9*(11), 4185–4208. doi: 10.5194/gmd-9-4185-2016

Heuzé, C. (2021). Antarctic Bottom Water and North Atlantic Deep Water in CMIP6 models. *Ocean Science*, *17*(1), 59–90. doi: 10.5194/os-17-59-2021

Hirschi, J. J., Barnier, B., Böning, C., Biastoch, A., Blaker, A. T., Coward, A., ... Xu, X. (2020). The Atlantic Meridional Overturning Circulation in High-Resolution Models. *Journal of Geophysical Research: Oceans*, *125*(4), e2019JC015522. doi: 10.1029/2019JC015522

Jackson, L. C., Roberts, M. J., Hewitt, H. T., Iovino, D., Koenigk, T., Meccia, V. L., ... Wood, R. A. (2020). Impact of ocean resolution and mean state on the rate of AMOC weakening. *Climate Dynamics*, *55*(7), 1711–1732. doi: 10.1007/s00382-020-05345-9

Johnson, H. L., Cessi, P., Marshall, D. P., Schloesser, F., & Spall, M. A. (2019). Recent Contributions of Theory to Our Understanding of the Atlantic Meridional Overturning Circulation. *Journal of Geophysical Research: Oceans*, *124*(8),

5376–5399. doi: 10.1029/2019JC015330

Koldunov, N. V., Aizinger, V., Rakowsky, N., Scholz, P., Sidorenko, D., Danilov, S., & Jung, T. (2019). Scalability and some optimization of the Finite-volumE Sea ice–Ocean Model, Version 2.0 (FESOM2). *Geoscientific Model Development*, *12*(9), 3991–4012. doi: 10.5194/gmd-12-3991-2019

Kwon, Y.-O., & Frankignoul, C. (2014). Mechanisms of Multidecadal Atlantic Meridional Overturning Circulation Variability Diagnosed in Depth versus Density Space. *Journal of Climate*, *27*(24), 9359–9376. doi: 10.1175/JCLI-D-14-00228.1

Liu, W., Xie, S.-P., Liu, Z., & Zhu, J. (2017). Overlooked possibility of a collapsed Atlantic Meridional Overturning Circulation in warming climate. *Science Advances*, *3*(1), e1601666. doi: 10.1126/sciadv.1601666

Lozier, M. S., Bacon, S., Bower, A. S., Cunningham, S. A., Jong, M. F. d., Steur, L. d., ... Zika, J. D. (2017). Overturning in the Subpolar North Atlantic Program: A New International Ocean Observing System. *Bulletin of the American Meteorological Society*, *98*(4), 737–752. doi: 10.1175/BAMS-D-16-0057.1

Lozier, M. S., Li, F., Bacon, S., Bahr, F., Bower, A. S., Cunningham, S. A., ... Zhao, J. (2019). A sea change in our view of overturning in the subpolar North Atlantic. *Science*, *363*(6426), 516–521. doi: 10.1126/science.aau6592

Marson, J. M., Wainer, I., Mata, M. M., & Liu, Z. (2014). The impacts of deglacial meltwater forcing on the South Atlantic Ocean deep circulation since the Last Glacial Maximum. *Climate of the Past*, *10*(5), 1723–1734. doi: 10.5194/cp-10-1723-2014

Matos, F. D. A. O., Pereira, J., & Dengler, M. (2020). Salinity Biases and the Variability of the Atlantic Meridional Overturning Circulation in GFDL-CM3. *Ocean Science Journal*, *55*(4), 505–520. doi: 10.1007/s12601-020-0040-8

Matos, F. D. A. O., Sidorenko, D., Gierz, P., Shi, X., Ackermann, L., & Lohmann, G. (2022). *z- and ρ-amoc variability under pre-industrial, historical and abrupt4xco$_2$ climates in awi-esm2.1* [dataset]. Zenodo. doi: 10.5281/zenodo.6992810

McCarthy, G., Smeed, D., Cunningham, S., & Roberts, C. (2017). Atlantic Meridional Overturning Circulation. In M. Frost, I. Baxter, P. Buckley, S. Dye, & B. D. Stocker (Eds.), *MCCIP Review 2017* (pp. 15–21). Lowestoft: Marine climate change impacts partnership. doi: 10.14465/2017.arc10.002-atl

Mecking, J., Drijfhout, S., Jackson, L., & Andrews, M. (2017). The effect of model bias on Atlantic freshwater transport and implications for AMOC bi-stability. *Tellus A: Dynamic Meteorology and Oceanography*, *69*(1), 1299910. doi: 10.1080/16000870.2017.1299910

Megann, A. (2018). Estimating the numerical diapycnal mixing in an eddy-permitting ocean model. *Ocean Modelling*, *121*, 19–33. doi: 10.1016/j.ocemod.2017.11.001

Meinen, C. S., Speich, S., Piola, A. R., Ansorge, I., Campos, E., Kersalé, M., ... Garzoli, S. L. (2018). Meridional Overturning Circulation Transport Variability at 34.5°S During 2009–2017: Baroclinic and Barotropic Flows and the Dueling Influence of the Boundaries. *Geophysical Research Letters*, *45*(9), 4180–4188. doi: 10.1029/2018GL077408

Petersen, M. R., Jacobsen, D. W., Ringler, T. D., Hecht, M. W., & Maltrud, M. E. (2015). Evaluation of the arbitrary Lagrangian–Eulerian vertical coordinate method in the MPAS-Ocean model. *Ocean Modelling*, *86*, 93–113. doi: 10.1016/j.ocemod.2014.12.004

Rackow, T., Goessling, H. F., Jung, T., Sidorenko, D., Semmler, T., Barbi, D., & Handorf, D. (2018). Towards multi-resolution global climate modeling with ECHAM6-FESOM. Part II: climate variability. *Climate Dynamics*, *50*(7), 2369–2394. doi: 10.1007/s00382-016-3192-6

Raddatz, T. J., Reick, C. H., Knorr, W., Kattge, J., Roeckner, E., Schnur, R., ... Jungclaus, J. (2007). Will the tropical land biosphere dominate the climate–carbon cycle feedback during the twenty-first century? *Climate Dynamics*, *29*(6), 565–574. doi: 10.1007/s00382-007-0247-8

Reintges, A., Martin, T., Latif, M., & Keenlyside, N. S. (2017). Uncertainty in twenty-first century projections of the Atlantic Meridional Overturning Circulation in CMIP3 and CMIP5 models. *Climate Dynamics*, *49*(5), 1495–1511. doi: 10.1007/s00382-016-3180-x

Roberts, M. J., Jackson, L. C., Roberts, C. D., Meccia, V., Docquier, D., Koenigk, T., ... Wu, L. (2020). Sensitivity of the Atlantic Meridional Overturning Circulation to Model Resolution in CMIP6 HighResMIP Simulations and Implications for Future Changes. *Journal of Advances in Modeling Earth Systems*, *12*(8), e2019MS002014. doi: 10.1029/2019MS002014

Rühs, S., Schwarzkopf, F. U., Speich, S., & Biastoch, A. (2019). Cold vs. warm water route – sources for the upper limb of the Atlantic Meridional Overturning Circulation revisited in a high-resolution ocean model. *Ocean Science*, *15*(3), 489–512. doi: 10.5194/os-15-489-2019

Santoso, A., & England, M. H. (2004). Antarctic Intermediate Water Circulation and Variability in a Coupled Climate Model. *Journal of Physical Oceanography*, *34*(10), 2160–2179. doi: 10.1175/1520-0485(2004)034⟨2160:AIWCAV⟩2.0.CO;2

Saunders, P. M. (2001). The dense northern overflows. In G. Siedler, J. Church, & J. Gould (Eds.), *Ocean Circulation and Climate* (Vol. 77, pp. 401–417). Academic Press. doi: 10.1016/S0074-6142(01)80131-5

Scholz, P., Sidorenko, D., Danilov, S., Wang, Q., Koldunov, N., Sein, D., & Jung, T. (2022). Assessment of the Finite-VolumE Sea ice–Ocean Model (FESOM2.0) – Part 2: Partial bottom cells, embedded sea ice and vertical mixing library CVMix. *Geoscientific Model Development*, *15*(2), 335–363. doi: 10.5194/gmd-15-335-2022

Scholz, P., Sidorenko, D., Gurses, O., Danilov, S., Koldunov, N., Wang, Q., ... Jung, T. (2019). Assessment of the Finite-volumE Sea ice-Ocean Model (FESOM2.0) – Part 1: Description of selected key model elements and comparison to its predecessor version. *Geoscientific Model Development*, *12*(11), 4875–4899. doi: 10.5194/gmd-12-4875-2019

Sein, D. V., Koldunov, N. V., Danilov, S., Sidorenko, D., Wekerle, C., Cabos, W., ... Jung, T. (2018). The Relative Influence of Atmospheric and Oceanic Model Resolution on the Circulation of the North Atlantic Ocean in a Coupled Climate Model. *Journal of Advances in Modeling Earth Systems*, *10*(8), 2026–2041. doi: 10.1029/2018MS001327

Sévellec, F., & Fedorov, A. V. (2016). AMOC sensitivity to surface buoyancy fluxes: Stronger ocean meridional heat transport with a weaker volume transport? *Climate Dynamics*, *47*(5), 1497–1513. doi: 10.1007/s00382-015-2915-4

Sévellec, F., Fedorov, A. V., & Liu, W. (2017). Arctic sea-ice decline weakens the Atlantic Meridional Overturning Circulation. *Nature Climate Change*, *7*(8), 604–610. doi: 10.1038/nclimate3353

Shi, X., Lohmann, G., Sidorenko, D., & Yang, H. (2020, July). Early-Holocene simulations using different forcings and resolutions in AWI-ESM. *The Holocene*, *30*(7), 996–1015. doi: 10.1177/0959683620908634

Sidorenko, D., Danilov, S., Fofonova, V., Cabos, W., Koldunov, N., Scholz, P., ... Wang, Q. (2020). AMOC, Water Mass Transformations, and Their Responses to Changing Resolution in the Finite-VolumE Sea Ice-Ocean Model. *Journal of Advances in Modeling Earth Systems*, *12*(12), e2020MS002317. doi: 10.1029/2020MS002317

Sidorenko, D., Danilov, S., Koldunov, N., Scholz, P., & Wang, Q. (2020). Simple algorithms to compute meridional overturning and barotropic streamfunctions

on unstructured meshes. *Geoscientific Model Development*, *13*(7), 3337–3345. doi: 10.5194/gmd-13-3337-2020

Sidorenko, D., Danilov, S., Streffing, J., Fofonova, V., Goessling, H. F., Scholz, P., ... Jung, T. (2021). AMOC Variability and Watermass Transformations in the AWI Climate Model. *Journal of Advances in Modeling Earth Systems*, *13*(10), e2021MS002582. doi: 10.1029/2021MS002582

Sidorenko, D., Goessling, H., Koldunov, N., Scholz, P., Danilov, S., Barbi, D., ... Jung, T. (2019). Evaluation of FESOM2.0 Coupled to ECHAM6.3: Preindustrial and HighResMIP Simulations. *Journal of Advances in Modeling Earth Systems*, *11*(11), 3794–3815. doi: 10.1029/2019MS001696

Sidorenko, D., Rackow, T., Jung, T., Semmler, T., Barbi, D., Danilov, S., ... Wang, Q. (2015). Towards multi-resolution global climate modeling with ECHAM6–FESOM. Part I: model formulation and mean climate. *Climate Dynamics*, *44*(3), 757–780. doi: 10.1007/s00382-014-2290-6

Speer, K., Rintoul, S. R., & Sloyan, B. (2000). The Diabatic Deacon Cell. *Journal of Physical Oceanography*, *30*(12), 3212–3222. doi: 10.1175/1520-0485(2000)030⟨3212:TDDC⟩2.0.CO;2

Srokosz, M., Baringer, M., Bryden, H., Cunningham, S., Delworth, T., Lozier, S., ... Sutton, R. (2012). Past, Present, and Future Changes in the Atlantic Meridional Overturning Circulation. *Bulletin of the American Meteorological Society*, *93*(11), 1663–1676. doi: 10.1175/BAMS-D-11-00151.1

Stevens, B., Giorgetta, M., Esch, M., Mauritsen, T., Crueger, T., Rast, S., ... Roeckner, E. (2013). Atmospheric component of the MPI-M Earth System Model: ECHAM6. *Journal of Advances in Modeling Earth Systems*, *5*(2), 146–172. doi: 10.1002/jame.20015

Stevens, D. P., & Ivchenko, V. O. (1997). The zonal momentum balance in an eddy-resolving general-circulation model of the southern ocean. *Quarterly Journal of the Royal Meteorological Society*, *123*(540), 929–951. doi: 10.1002/qj.49712354008

Stommel, H. (1961). Thermohaline Convection with Two Stable Regimes of Flow. *Tellus*, *13*(2), 224–230. doi: 10.1111/j.2153-3490.1961.tb00079.x

Stouffer, R. J., Eyring, V., Meehl, G. A., Bony, S., Senior, C., Stevens, B., & Taylor, K. E. (2017). CMIP5 Scientific Gaps and Recommendations for CMIP6. *Bulletin of the American Meteorological Society*, *98*(1), 95–105. doi: 10.1175/BAMS-D-15-00013.1

Valcke, S. (2013). The OASIS3 coupler: a European climate modelling community software. *Geoscientific Model Development*, *6*(2), 373–388. doi: 10.5194/gmd-6-373-2013

Weijer, W., Cheng, W., Garuba, O. A., Hu, A., & Nadiga, B. T. (2020). CMIP6 Models Predict Significant 21st Century Decline of the Atlantic Meridional Overturning Circulation. *Geophysical Research Letters*, *47*(12), e2019GL086075. doi: 10.1029/2019GL086075

Xu, X., Chassignet, E. P., & Wang, F. (2019). On the variability of the Atlantic meridional overturning circulation transports in coupled CMIP5 simulations. *Climate Dynamics*, *52*(11), 6511–6531. doi: 10.1007/s00382-018-4529-0

Xu, X., Rhines, P. B., & Chassignet, E. P. (2018). On Mapping the Diapycnal Water Mass Transformation of the Upper North Atlantic Ocean. *Journal of Physical Oceanography*, *48*(10), 2233–2258. doi: 10.1175/JPO-D-17-0223.1